JOURNAL OF SPACECRAFT AND ROCKETS
Vol. 32, No. 4, July–August 1995

# Redesign of the Celestial Pointing Cone Control Gains for the Galileo Spacecraft

Che-Hang Charles Ih* and Kathryn B. Hilbert†
*Jet Propulsion Laboratory, California Institute of Technology, Pasadena, California 91109*

**During September and October 1991, pictures of the Gaspra asteroid and neighboring stars were taken by the Galileo Optical Navigation Team for the purpose of navigating the Galileo spacecraft for a successful Gaspra encounter. The star tracks in these pictures showed that the scan-platform celestial-pointing cone controller performed poorly in compensating for wobble-induced cone offsets. This poor performance is attributed to the very conservative cone-control gains selected before launch. Thus the cone-control gains were redesigned. The simulation results, the in-flight confirmation test, and the more recent optical-navigation pictures of the Ida asteroid all indicated that tremendous improvement in the scan-platform performance in compensating for the cone offsets has been achieved using the new gains, at no additional cost of the control torque.**

## Nomenclature

GM = gain margin
$I$ = scan-platform moment of inertia about the cone axis
$K_P$ = position gain
$K_d$ = rate gain
PLD = negative of lead-filter pole
PM = phase gain
$T$ = sampling period, $66\frac{2}{3}$ ms
TF = system open-loop transfer function
$TF_P$ = transfer function for the continuous rigid-body plant (scan platform) and gyro with a sampler and zero-order hold
ZLD = negative of lead-filter zero
$\zeta$ = system closed-loop damping ratio
$\theta$ = cone angular position
$\dot{\theta}$ = cone angular rate
$\omega$ = system closed-loop bandwidth

## Introduction

The dual-spin Galileo spacecraft was launched in October 1989 and is on its way to Jupiter to explore the planet and its moons. A sketch of the spacecraft is shown in Fig. 1. The scan platform is attached to the stator (despun section), which is in turn attached to the rotor (spun section) of the spacecraft. There are two degrees of freedom for controlling the inertial orientation of the scan platform. The cone actuator controls the relative position between the platform and the stator about the cone axis. The resulting motion, seen in a picture, is called the cone motion. Another degree of freedom is provided by the clock actuator, which controls the relative position between the rotor and the stator about the clock axis. The clock motion can be translated into the cross-cone motion (perpendicular to the cone motion) in a picture. The cone and clock axes are perpendicular to one another so that the platform may be gimbaled in two orthogonal directions. The clock actuator is also referred to as the spin bearing assembly (SBA) actuator, and the cone actuator as the scan articulation subsystem (SAS) actuator.

Control of the scan platform is implemented by executing the cone and clock control algorithms every $66\frac{2}{3}$ ms in the onboard computer.

Received July 11, 1994; revision received Nov. 29, 1994; accepted for publication Dec. 2, 1994. 

*Member of Technical Staff, Automation and Control Section, 4800 Oak Grove Drive. Member AIAA.
†Technical Group Supervisor, Automation and Control Section, 4800 Oak Grove Drive.

There are five scan-platform pointing methods,[1] as shown in Table 1. Among them, the celestial pointing method in inertial mode is the prime mode for science data collection, since it provides the greatest accuracy. The reason is that in this mode, gyros (mounted on the scan platform) are used to determine the platform attitude directly. Gyros have much higher accuracy than the SAS and SBA optical encoders. Also, gyros can sense the spacecraft motions (wobble, etc.) in the inertial frame, thus allowing these motions to be compensated by the controllers. The details of the design of cone and clock controllers are presented in Ref. 1. Since the problem investigated in this paper is about the cone controller, only the cone controller will be discussed in the following sections.

Long-exposure optical-navigation (OPNAV) pictures of Gaspra and surrounding stars were taken using the solid-state imaging (SSI) camera during September and October 1991 for the purpose of navigating the spacecraft for a successful Gaspra encounter. Unusual star tracks were observed in those pictures. Among them, the OPNAV 5 picture (Fig. 2; picture frame size was 8.128 by 8.128 mrad) had drawn special interest. It involved four 0.57-mrad slews in cross-cone with the spacecraft in inertial mode. The approximate wobble (defined as the angle between the spacecraft principal axis and the SBA axis shown in Fig. 1), estimated using rotor right ascension (RA) and declination (DEC) telemetry, was 0.54 mrad. Ideally, the SSI image should have consisted of four equal straight line segments in the cross-cone direction. However, while the wobble effect was well compensated in cross-cone, a large cone offset was observed (the worst offset was about 0.5 mrad, whereas the prelaunch

**Table 1 Pointing methods[1] for Galileo scan-platform control**

| Pointing method | Spacecraft configuration | AACS modes | Attitude sensor |
|---|---|---|---|
| Celestial pointing (with or without strip generation) | Dual spin | Cruise | Star scanner optical encoders |
| | | Inertial | Star scanner optical encoder gyros |
| Stator pointing (caged cone and celestial clock) | Dual spin | Cruise | Star scanner optical encoders |
| | | Inertial | Star scanner optical encoder gyros |
| Caged cone, caged clock | All spin | All spin | Optical encoders |
| Caged cone, clock-commanded spin | All spin<br>Dual spin<br>Transition | All spin<br>Cruise<br>Inertial<br>Transition | Optical encoders |

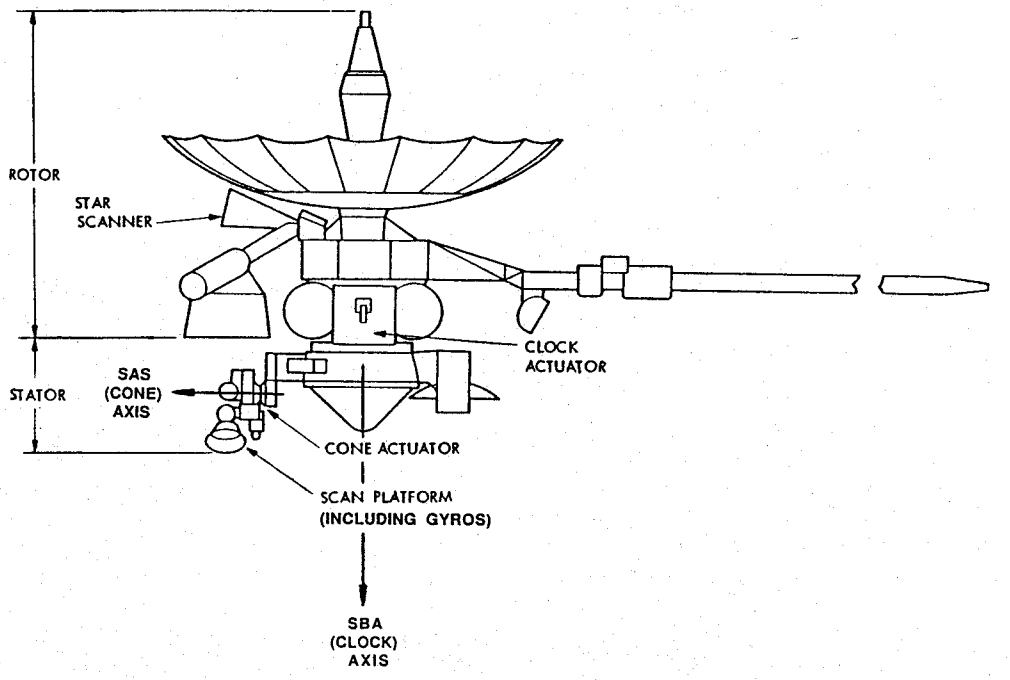


**Fig. 1 Galileo spacecraft.**

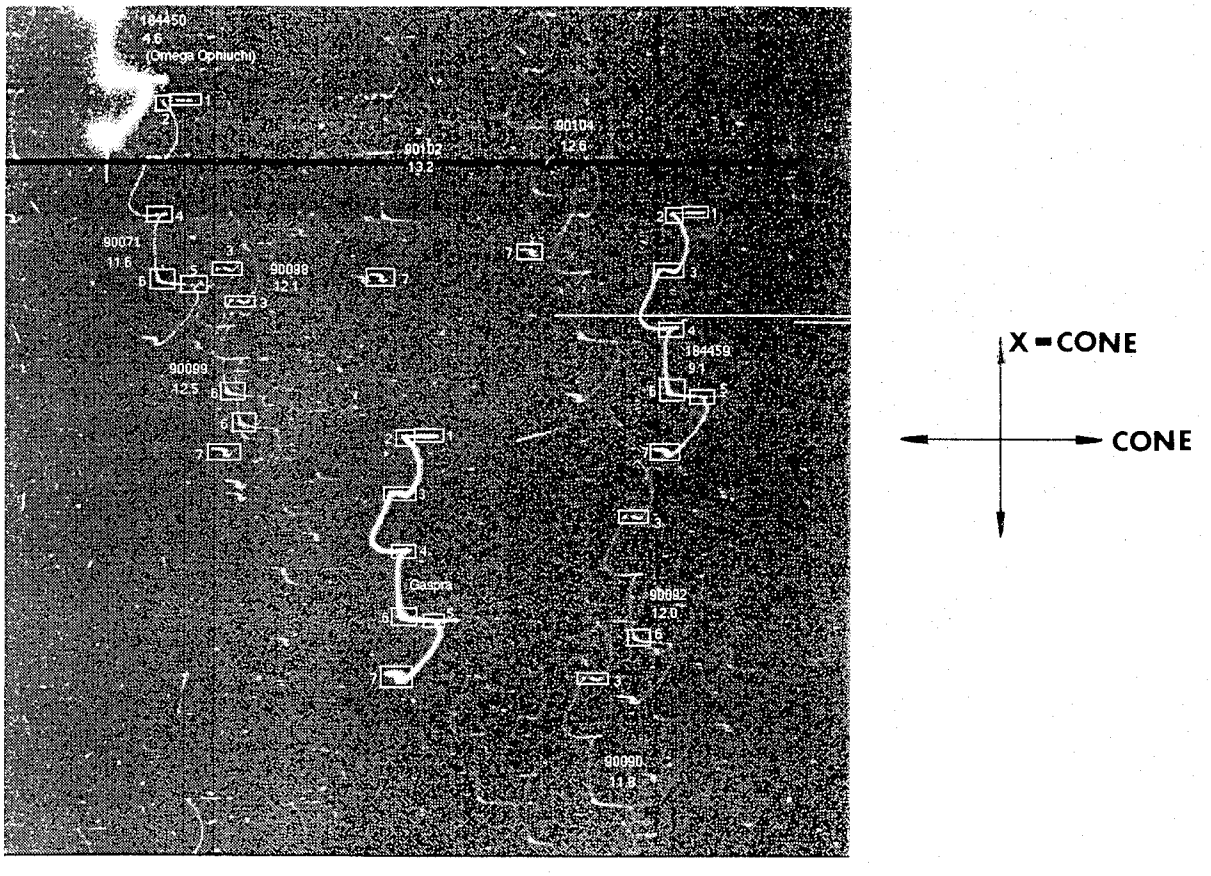


**Fig. 2 Gaspra OPNAV 5 picture.**

pointing requirement[1] is 0.14 mrad). The cone offset continued to increase until the commanded control torque was large enough to overcome the friction and move the scan platform to compensate for the cone errors.

The OPNAV 5 cone-controller performance was recreated using a Galileo ground software simulation tool called FUNSIM. The wobble and cone actuator friction conditions set up for this simulated OPNAV 5 were very close to those in flight. The wobble for the simulated OPNAV 5 was 0.57 mrad. Note how similar the slew pattern of the simulated OPNAV 5 (Fig. 3) is to that of the real OPNAV 5 picture (Fig. 2). The cone-controller performance shown in Fig. 3 is used as the baseline for comparison with other simulation cases.

This poor cone performance is not surprising, because very conservative control gains were selected before launch, based on their high stability margins. These gains were intended to be updated once sufficient in-flight scan-platform data became available.

The cone-control gains were then redesigned with the aid of the MATLAB control system analysis tools, and simulation results demonstrated that excellent cone performance was achievable under various slew and friction conditions with sufficient stability margins. These new gains were then uplinked and tested on the spacecraft. The test results demonstrated that substantial improvement in the cone offset has been achieved at no additional cost of the control torque. The more recent OPNAV pictures of Ida and surrounding stars further confirmed the performance improvements for the inertial-mode celestial-pointing cone controller in compensating for the cone offsets.

## Redesign of Inertial-Mode Celestial-Pointing Cone-Control Gains

### Controller Structure

A block diagram[2] of the inertial-mode celestial-pointing cone-control system is shown in Fig. 4. What is not shown in the diagram is the scan commander. The scan commander processes the scan-platform slew commands to determine the commanded position of the platform and the corresponding slew paths. In order to avoid exciting the flexible stator structure, the scan commander generates smooth feedforward torque profiles for the two actuators,[3] as shown in Fig. 4. The cone controller consists of a proportional plus derivative (PD) controller, a lead filter, and the disturbance estimator. The lead filter was designed so that the control-loop bandwidth and the response of the system to the expected type of behavior were optimized. For example, step position or rate errors are not expected to occur because the scan commander generates smooth position, rate, and torque profiles as mentioned. Because it is unlikely that there will be any large position or rate overshoots, the controller can be made underdamped.[2] The disturbance estimator is used to compensate for the friction in the cone actuator. Details of the disturbance estimator can be found in Ref. 4. The gyro integrator has two rate estimators. One is used during the period of low acceleration, the other for high acceleration. The system with the low rate estimator (Fig. 4) is used to drive the control gains, since it is the one used most of the time.

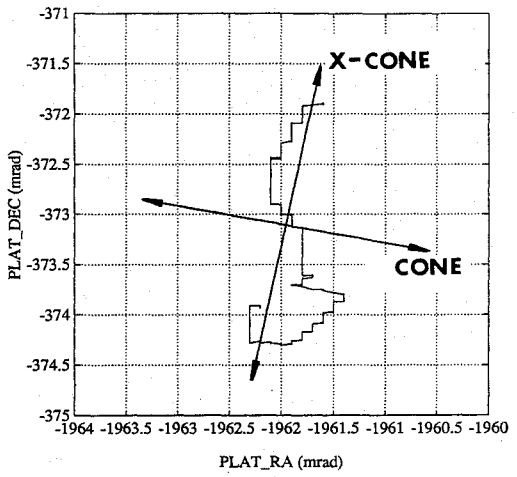


**Fig. 3 Scan-platform attitudes for simulated OPNAV 5 using old (conservative) cone-control gains.**

The $z$ transform of the system open-loop transfer function is

$$\mathrm{TF} = \left[\left(K_P + \frac{K_d(z-1)}{Tz}\right)\frac{z+\mathrm{ZLD}}{z+\mathrm{PLD}} + \frac{I}{T^2}\frac{z^2-2z+1}{z^2}\right] \times \frac{2z^2}{2z^3-z-1}\mathrm{TF}_P$$

The block diagram for $\mathrm{TF}_p$ in the $s$ domain is show below:

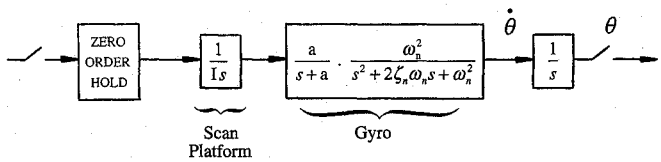


and the $z$ transform of $\mathrm{TF}_p$ is

$$\mathrm{TF}_P = (1.0298097\times10^{-3}z^4 + 3.16833094\times10^{-3}z^3 + 2.44151548\times10^{-4}z^2 + 1.45408419\times10^{-6}z + 1.26839432\times10^{-8}) \times [I(z^5 - 2.0004z^4 + 1.00106z^3 - 9.0333\times10^{-4}z^2 + 2.5017\times10^{-4}z - 3.78247\times10^{-8})]^{-1}$$

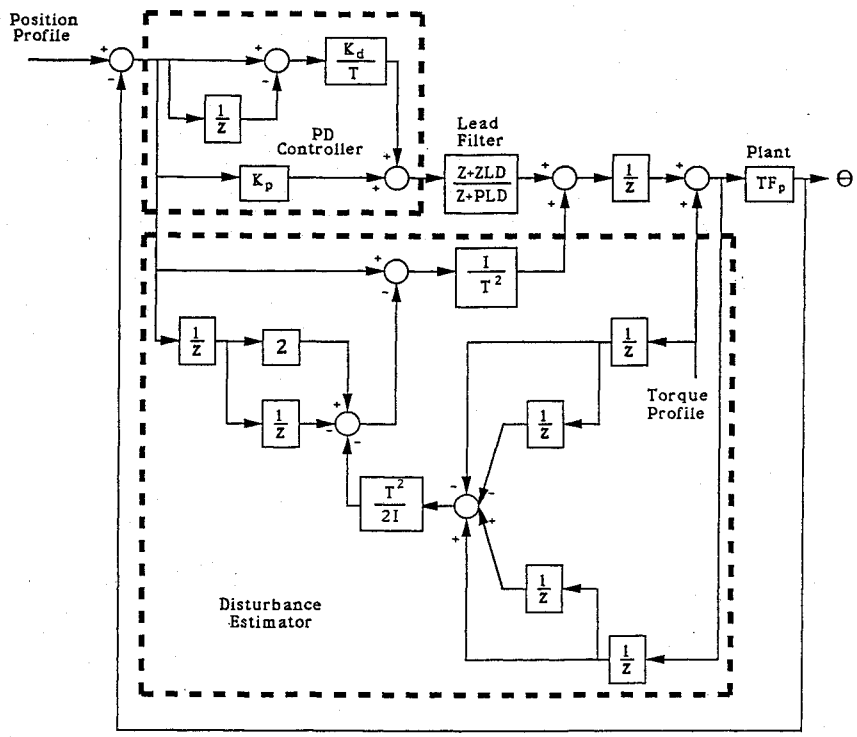


**Fig. 4 Block diagram of the Galileo inertial-mode celestial-pointing cone-control system.**

**Original (Old) Cone-Control Gain Design**

In the original design, the pole placement technique and MACSYMA functions were used to derive the control gains $K_P$ and $K_d$, and two sets of control gains were designed. The conservative set has high stability margins and low performance, whereas the nonconservative set has low stability margins and high performance. As mentioned before, the conservative control law was the one that had been used since launch, for stability reasons. The gains, bandwidth, damping ratio, phase margin, and gain margin for the conservative and nonconservative control laws are listed as:

| Conservative control law | Nonconservative control law |
|---|---|
| $K_{PC} = 19.69\,\text{N}\cdot\text{m/rad}$ | $K_{PN} = 116.687\,\text{N}\cdot\text{m/rad}$ |
| $K_{dC} = 11.94\,\text{N}\cdot\text{m}\cdot\text{s/rad}$ | $K_{dN} = 33.573\,\text{N}\cdot\text{m}\cdot\text{s/rad}$ |
| $\omega = 0.25\,\text{Hz}$ | $\omega = 0.85\,\text{Hz}$ |
| $\zeta = 0.4$ | $\zeta = 0.4$ |
| PM = 40 deg | PM = 15 deg |
| GM = 5.53 dB(1.89) | GM = 3.86 dB(1.56) |

Since there is a tradeoff between the performance and stability of the controller, the new set of control gains should be somewhere in between these two extremes.

**New Cone-Control Gain Design**

The pole placement technique used by the original designer for deriving the control gains starts by placing the dominant closed-loop poles at the appropriate locations in the $s$ plane to achieve the desired bandwidth and damping ratio. Given the ideal characteristic equation and the characteristic equation containing the unknown gains, a set of simultaneous equations can be formed by equating the corresponding coefficients of the two characteristic equations. Symbolic manipulation tools like MACSYMA can then be used to solve for the gains. The stability margins are then checked via Bode plots by substituting the control gains into the open-loop transfer function. If the stability margins are not acceptable, the dominant poles are relocated and the whole process is repeated. Since this iterative process is very tedious and time-consuming, a more systematic design approach was adopted to design the new gains. Namely, the control gains were varied through a certain range that encompassed both the conservative and nonconservative gains, and the corresponding gain margin, phase margin, bandwidth, and damping ratio for each set of gains were then calculated. The three-dimensional mesh surfaces of gain and phase margins versus normalized gains, $K_P/K_{PC}$ and $K_d/K_{dC}$ were generated by MATLAB and are shown in Fig. 5, where $K_{PC}$ and $K_{dC}$ are the conservative position and rate gains,

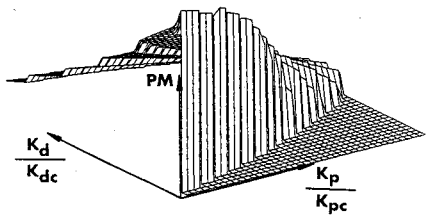


a) Phase margin

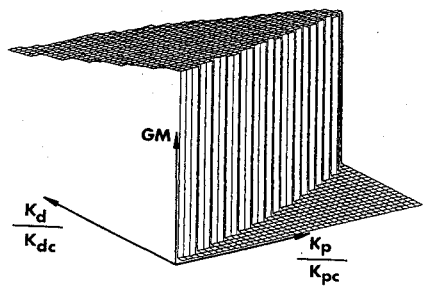


b) Gain margin

**Fig. 5 Mesh surfaces of gain and phase margins as a function of normalized position and rate gains.**

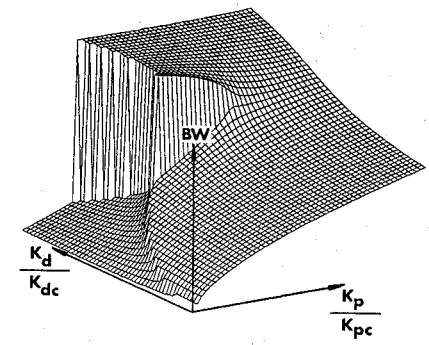


a) Closed-loop bandwidth

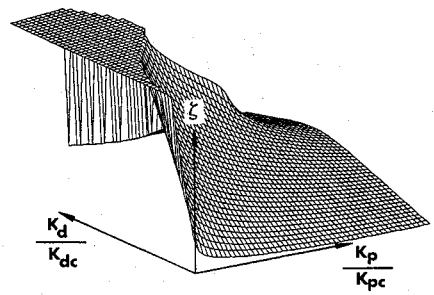


b) Closed-loop damping ratio

**Fig. 6 Mesh surfaces of closed-loop bandwidth and damping ratio as a function of normalized position and rate gains.**

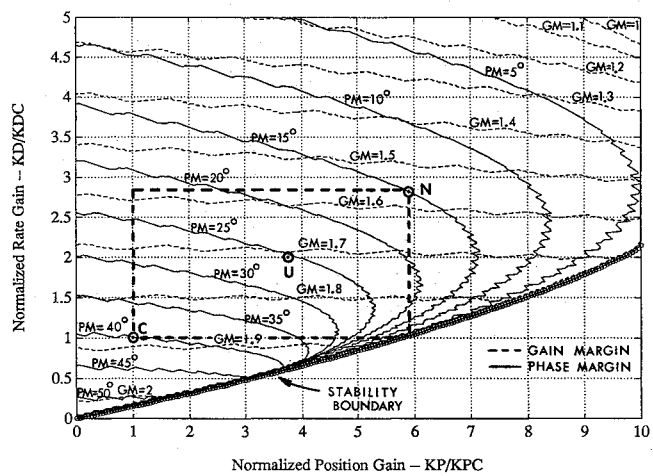


**Fig. 7 Contours of constant gain and phase margins as a function of normalized position and rate gains.**

respectively. As expected, the higher the gains, the lower the stability margins. The mesh surfaces of the closed-loop bandwidth and damping ratio are shown in Fig. 6. Also as expected, the higher the gains, the higher the bandwidth; the higher the rate gain, the higher the damping ratio. The tradeoff between the performance and stability is obvious from these plots.

By slicing these mesh surfaces horizontally at different heights, contours of constant gain margin, phase margin, bandwidth, and damping ratio can be obtained. The function CONTOUR in MATLAB was designed for such purposes. The resulting contour plots of constant stability margins are shown in Fig. 7, and those of constant bandwidth and damping ratio are shown in Fig. 8. To the right of the stability boundary is the unstable region. The validity of those plots is verified by checking how well the old gains fit in them. By locating the conservative gains (point $C$) and nonconservative gains (point $N$) in Fig. 7 according to their gain values, one sees that the corresponding gain and phase margins are almost exactly the same as those listed previously. The bandwidth and damping ratio in Fig. 8 are slightly off. The reason is that all these curves were generated numerically. If the gains were varied at an infinitely fine increment, they would be exactly the same as the analytical results. However, finer increments of control gains require more computational time.

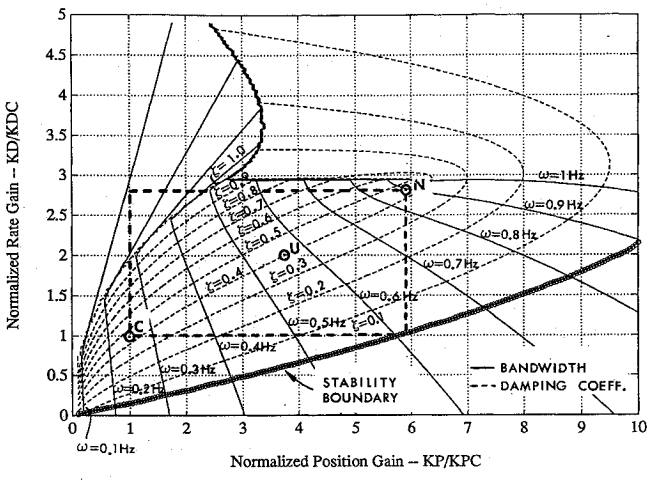


**Fig. 8 Contours of constant closed-loop bandwidth and damping ratio as a function of normalized position and rate gains.**

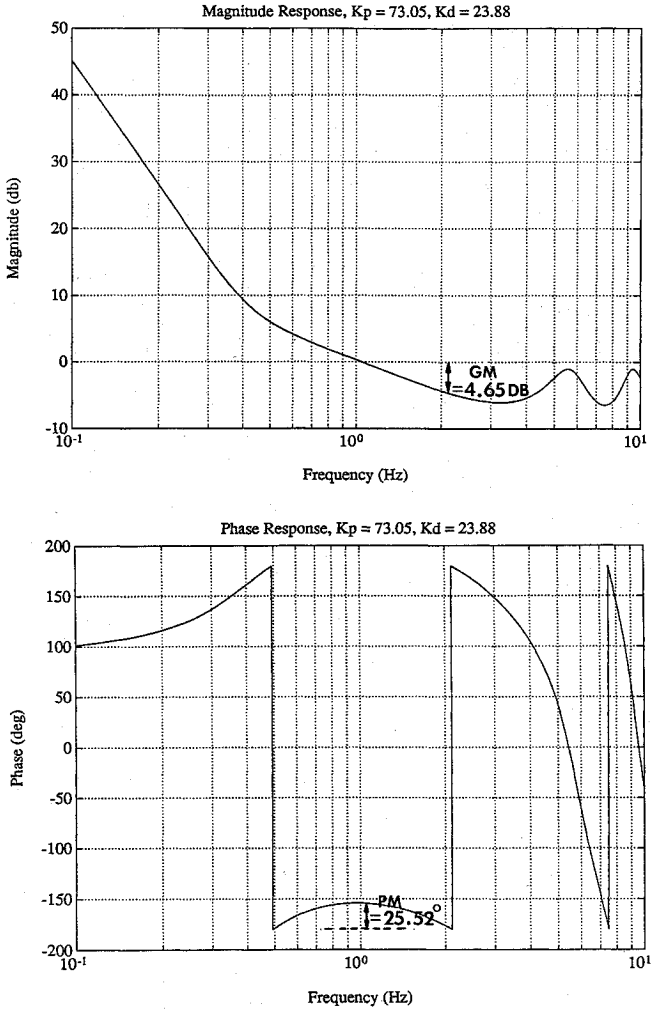


**Fig. 9 Stability margins of the inertial-mode celestial-pointing cone-control system with the new control gains.**

For the intended purpose of these plots as a general design guideline, they are accurate enough. Treating points $C$ and $N$ as the two ends of a diagonal, a rectangle can be drawn. The new gains (point $U$) should be within this rectangle.

The criterion used for selecting the new gains was as follows. Since both the conservative and nonconservative gains result in a closed-loop damping ratio of 0.4, it was desirable to maintain the same damping ratio. Hence point $U$ can be slid "up" from point $C$ along the $\zeta = 0.4$ curve. When it reaches $\omega = 0.56$ Hz, the phase margin reduces to about 25 deg, and the gain margin reduces to about 1.7. At this point, it was felt that the gains should not be increased any further, because sufficient stability margins are required to accommodate unmodeled nonlinearities. Once the nonlinear SAS friction is included, the stability margins will be a little lower. Based on where point $U$ is located in the contour plots, the new gains were calculated to be

$$K_p = 73.05\,\text{N} \cdot \text{m/rad}$$

$$K_d = 23.88\,\text{N} \cdot \text{m} \cdot \text{s/rad}$$

By substituting these new gains into the transfer function, the exact closed-loop bandwidth and damping ratio were found to be

$$\omega = 0.55 \text{ Hz}$$

$$\zeta = 0.372$$

By generating Bode plots with these new gains, the exact stability margins were obtained as

$$\text{GM} = 4.65\,\text{dB}(1.71)$$

$$\text{PM} = 25.52\,\text{deg}$$

as shown in Fig. 9. This combination is deemed to be optimal, considering all the tradeoffs.

## Performance Evaluation Through Simulation

The FUNSIM simulation of OPNAV 5 was rerun using the new cone-control gains. The result is shown in Fig. 10. All the initial conditions for the simulation remained the same as those used for obtaining the baseline performance in Fig. 3. The improvement in scan-platform slew performance can be immediately seen by comparing Figs. 3 and 10. The cone offset reduces substantially.

To further demonstrate the improvement in scan-platform performance for other small slews using the new cone-control gains, a sequence of scan-platform slew commands that had been executed on the spacecraft previously (called MINICAL 6) was used as a second test case in the FUNSIM simulations. The test involved nine slews—five in cone and four in cross-cone; each one was 7 mrad long. The result is shown in Fig. 11. Again, the improvement achieved by the new gains is obvious. For the latter half of the slew, the scan platform followed the desired path (dashed line) perfectly.

To examine the scan-platform performance for large and fast slews using the new cone-control gains, a 7SCAN command (used for repositioning the scan platform), which caused the scan platform to slew for more than 30 deg in cone (there was also a slew in clock) at a slew rate of 14.84 mrad/s, was simulated using FUNSIM. Superimposing the cone-position and scan-platform attitude time histories obtained using old and new gains showed that the difference between the two is indiscernible. This demonstrates that the

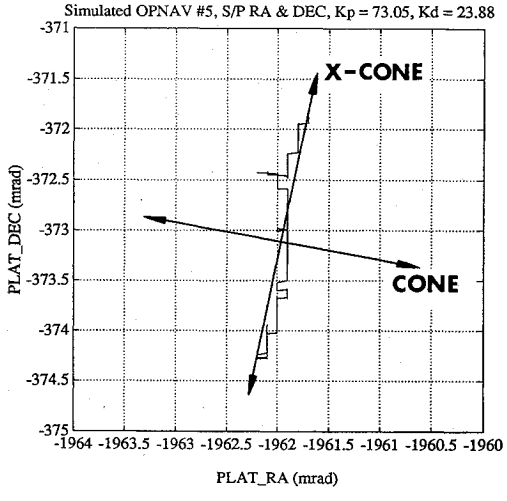


**Fig. 10 Scan-platform attitudes for simulated OPNAV 5 using new cone-control gains.**

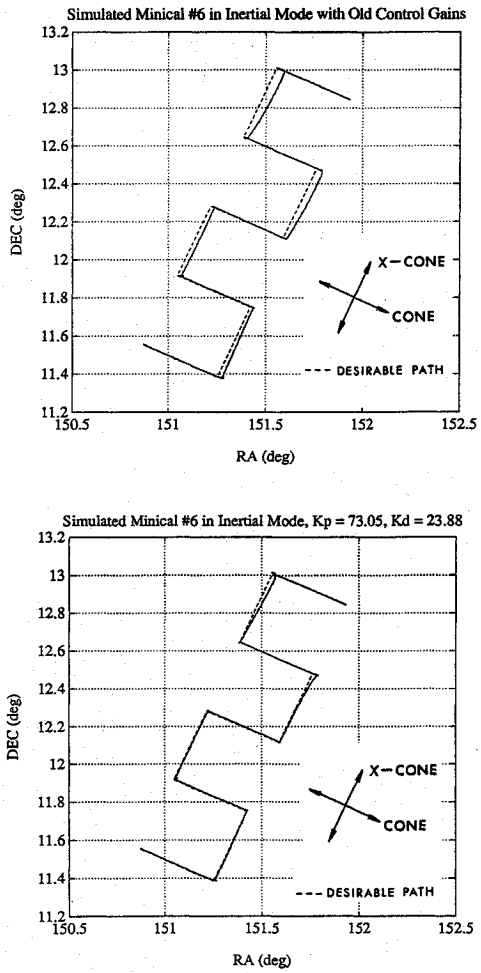


**Fig. 11 Scan-platform attitudes for simulated MINICAL 6 using a) old (conservative) and b) new cone-control gains.**

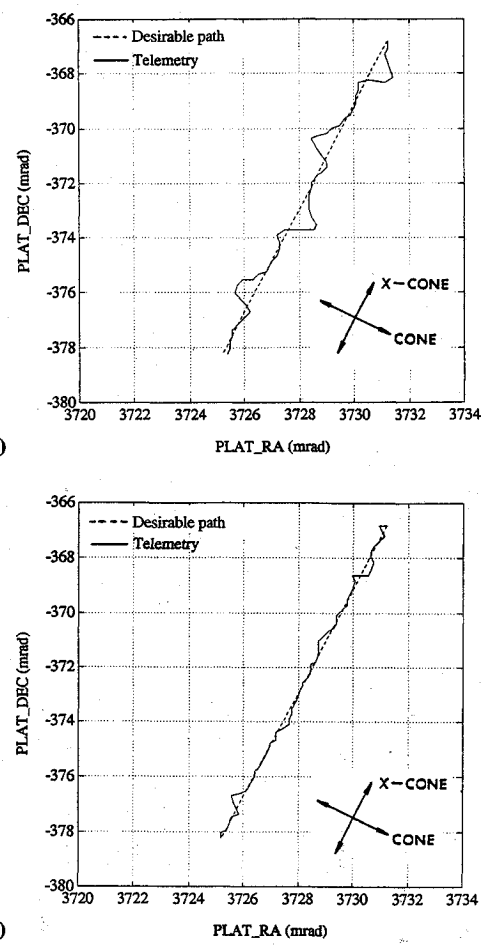


**Fig. 12 Scan platform RA vs DEC for the cross-cone slew at 124 deg SAS during the confirmation test: a) old gains and b) new gains.**

performance for large and fast slews has not been compromised with the new cone-control gains.

It is desirable to ensure that the new cone-control gains perform well at low SAS friction values. Thus the Coulomb friction coefficient in FUNSIM was cut down to one-quarter of its nominal value, and the OPNAV 5 FUNSIM simulation was rerun. The result showed no degradation in performance with the decreased SAS friction value.

## In-Flight Performance Verification

The new inertial-mode celestial-pointing cone-control gains were uplinked to the spacecraft, and the scan-platform performance has been closely monitored. Two representative cases are presented.

### Scan-Platform Performance Confirmation Test

A confirmation test was executed on the same day the new gains were uplinked. The estimated wobble on that day was about 1.1 mrad, which posed quite a challenge for celestial pointing. The test started with the old gains resident in the onboard software. After a series of test slews were completed using the old cone-control gains, the new gains were then patched into the code and the test was repeated. Identical slews were used for testing both the old gains and the new gains in order to directly compare the results. The sequence involved performing small cone (15.2 mrad) and cross-cone (8.7 mrad) slews at a low rate of 0.4 mrad/s at two separate cone positions, 124 and 145 deg. The reason these two cone positions were chosen is the relatively high Coulomb friction that had been measured there, leading to the worst operating conditions for the scan platform. For simplicity, only one typical result, the small cross-cone slew at 124 deg SAS, is presented here. The scan platform performance in cone can be best seen by examining the cone offsets during the cross-cone slews. The plots of scan-platform RA vs DEC for the cross-cone slew at 124 deg SAS with the old and new gains are shown in Fig. 12. The dashed line represents the desired scan-platform path generated using Galileo ground software. The significant improvement in cone offset is obvious. These tests also demonstrated that the scan-platform performance for large and fast slews has not been compromised with the new gains.

It was also found that the SAS torque required for achieving the better cone performance with the new gains was not higher than that for the old gains at all, as clearly manifested in Fig. 13. The reason is that although the new gains are higher, the cone position and rate errors are less. Thus the total torque is not higher.

### OPNAV Pictures for Ida Encounter

More recently (after the uplink of the new cone-control gains), OPNAV pictures of Ida and surrounding stars were taken for the purpose of navigating the spacecraft for an Ida encounter. All of these OPNAV pictures are similar; hence only OPNAV 2 is presented (Fig. 14) as an example. The wobble was about 0.56 mrad on the day it was taken. The sequence involved two 0.5-mrad cross-cone slews, followed by one combined cone and cross-cone slew (shown as the oblique line in Fig. 14), and then another two 0.5-mrad cross-cone slews. The frame size again was 8.128 by 8.128 mrad. It appeared in the picture that the magnitude of the first pair of cross-cone slews exceeded the magnitude of the second pair, and part of the second pair seemed to slew in the reverse direction. This was because that the scan platform was in the so-called "cone polar region" (150 deg $\leq \theta \leq$ 180 deg or 0 deg $\leq \theta \leq$ 30 deg) for this case. Since even a small cross-cone error results in large clock error in this region, for safety reasons the wobble-induced cross-cone error is not compensated by the clock controller. Hence, the wobble may lengthen, shorten, or even reverse the cross-cone slews. However, that is not a issue to be discussed in this paper. What is important is that excellent scan-platform cone performance is observed in the picture. The improvement in inertial-mode scan-platform perfor-

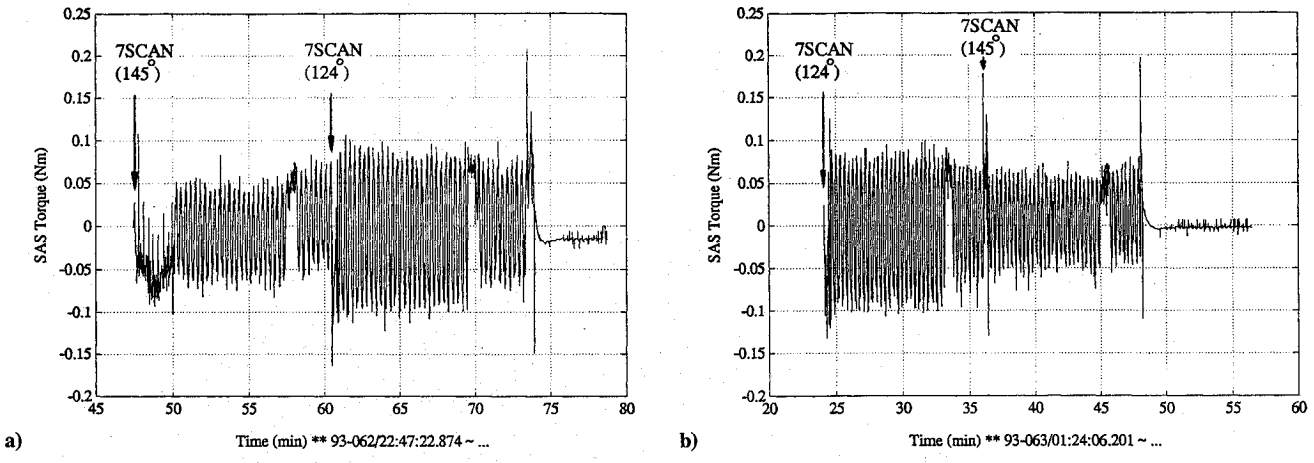


**Fig. 13 SAS torque time history during the confirmation test: a) old gains and b) new gains.**

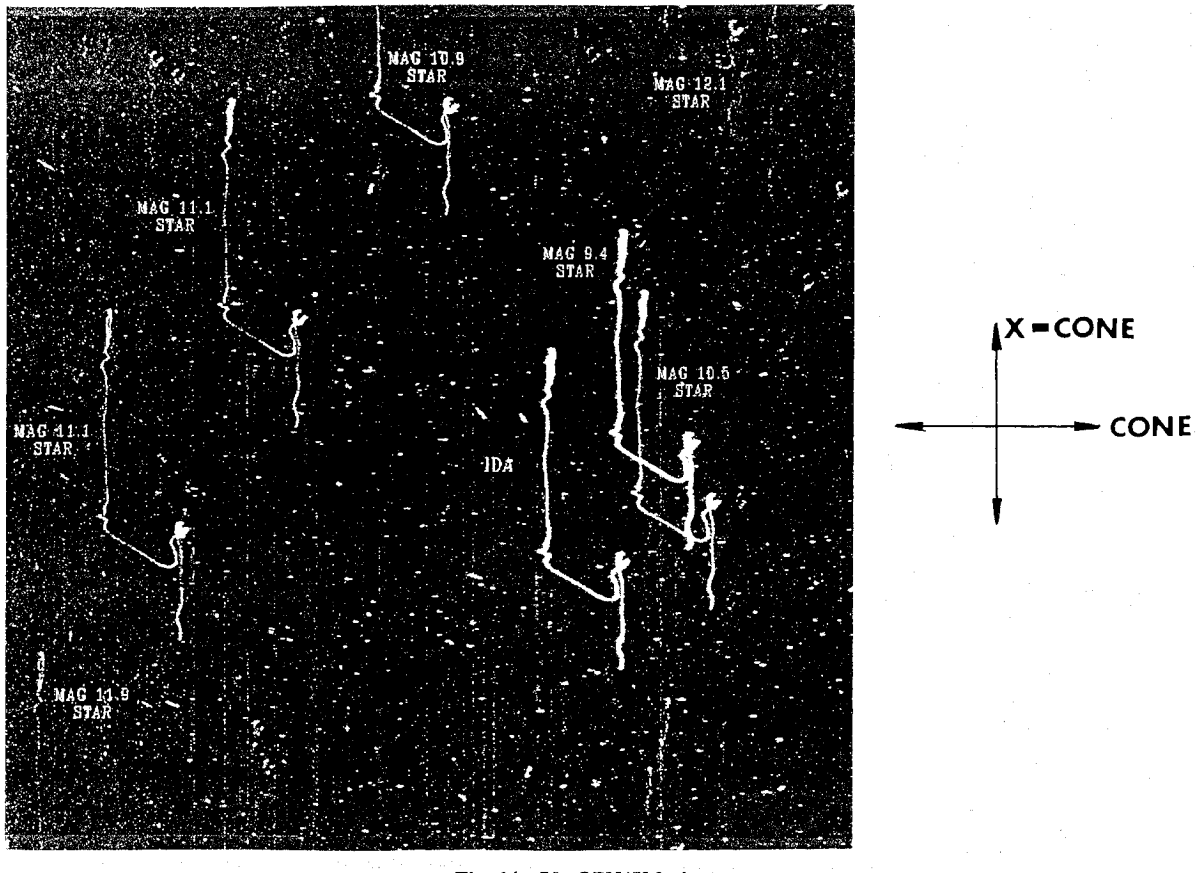


**Fig. 14 Ida OPNAV 2 picture.**

mance is evident in the comparison between Fig. 14 (Ida OPNAV 2) and Fig. 2 (Gaspra OPNAV 5).

## Conclusions

Motivated by the poor scan-platform performance observed in the Gaspra OPNAV 5 picture and the fact that conservative cone-control gains were selected before launch to assure sufficient stability margins, the Galileo inertial-mode celestial-pointing cone-control gains were redesigned. Tremendous improvement in scan-platform performance using the new gains has been demonstrated via FUNSIM simulations, in flight confirmation test, and recent Ida OPNAV pictures. Therefore, the new gains will be utilized for the rest of the Galileo mission.

## Acknowledgments

The research described in this paper was carried out at the Jet Propulsion Laboratory, California Institute of Technology, under contract with the National Aeronautics and Space Administration. The authors would like to thank Janis Chodas, Glenn Macala, and Gurkirpal Singh for their valuable discussions, and Gregory Harrison for developing the uplink sequence for the confirmation test.

## References

[1]Chodas, J. L., and Man, G. K., "Design of the Galileo Scan Platform Control," *Journal of Guidance, Control, and Dynamics*, Vol. 7, No. 4, 1984, pp. 422–429.

[2]Chodas, J. L., "Galileo Cone Controller Analysis and Algorithm Delivery for the 66 msec Rate group," Jet Propulsion Lab., internal memo EM 343-781, California Inst. of Technology, Pasadena, CA, Feb. 28, 1983.

[3]Man, G. K., and Breckenridge, W. G., "Command Profile for Galileo Scan Platform Control," American Astronomical Society, Paper 81-190, Aug. 1981.

[4]Chodas, J. L., "Friction Estimation Technique for Galileo Scan Platform Control," AIAA Paper 82-1458, Aug. 1982.

F. H. Lutze
*Associate Editor*